

Good flavor search in $SU(5)$: a machine learning approach

Fayez Abu-Ajamieh,^{1,*} Shinsuke Kawai,^{2,†} and Nobuchika Okada^{3,‡}

¹Formerly Center for High Energy Physics, Indian Institute of Science, Bangalore 560012, Karnataka, India

²Faculty of Science, Yamagata University, 1-4-12 Kojirakawa-machi, Yamagata, 990-8560 Japan

³Department of Physics and Astronomy, University of Alabama, Tuscaloosa, Alabama, AL35487 USA
(Dated: November 12, 2025)

We revisit the fermion mass problem of the $SU(5)$ grand unified theory using machine learning techniques. The original $SU(5)$ model proposed by Georgi and Glashow is incompatible with the observed fermion mass spectrum. Two remedies are known to resolve this discrepancy, one is through introducing a new interaction via a 45-dimensional field, and the other via a 24-dimensional field. We investigate which modification is more natural, defining naturalness as proximity to the original Georgi–Glashow $SU(5)$ model. Our analysis shows that, in both supersymmetric and non-supersymmetric scenarios, the model incorporating the interaction with the 24-dimensional field is more natural under this criterion. We then generalise these models by introducing a continuous parameter y , which takes the value 3 for the 45-dimensional field and 1.5 for the 24-dimensional field. Numerical optimisation reveals that $y \approx 0.8$ yields the closest match to the original $SU(5)$ model, indicating that this value corresponds to the most natural model according to our definition.

I. INTRODUCTION

Machine learning has become a key technology in modern scientific research, demonstrating utility also in theoretical investigations. Its application is particularly powerful when a theoretical model with a vast parameter space is confronted with extensive experimental data [1–3], or when the task involves classifying a large ensemble of theoretical models [4, 5]. Even in cases involving a moderately large number of parameters, such as in the Standard Model of particle physics, brute-force numerical analysis is often impeded by the curse of dimensionality, i.e., limitations in practical computational resources. In such cases, machine learning techniques have proven to be highly effective [6] (see also [7–10]).

We revisit the fermion mass problem in the context of grand unified theories (GUTs). The original $SU(5)$ GUT proposed by Georgi and Glashow [11], a prototypical framework for physics *beyond* the Standard Model, organizes the six quarks u, d, c, s, t, b and the six leptons $e, \mu, \tau, \nu_e, \nu_\mu, \nu_\tau$ into three families, each comprising the $\mathbf{10}$ and $\mathbf{\bar{5}}$ representations of the $SU(5)$ gauge group. This structure leads to the following mass relations at the GUT scale:

$$m_e = m_d, \quad m_\mu = m_s, \quad m_\tau = m_b. \quad (1)$$

Fermion mass predictions are then obtained via renormalisation group analysis, using these relations as boundary conditions. However, the resulting masses are incompatible with experimental observations; this discrepancy constitutes the fermion mass problem. One proposed solution involves a higher-dimensional operator that couples the fermions to the **24**-dimensional (adjoint) Higgs

field [12], referred to here as the 24-Higgs model. Another well-known approach introduces a Higgs field in the **45**-dimensional representation of $SU(5)$, which also couples to the fermions [13]; we refer to this as the 45-Higgs model. In both models, new (effective) Yukawa couplings are introduced, and by tuning the additional parametric degrees of freedom, the models can accommodate the observed fermion mass spectrum and flavour mixings.

While both of these approaches are theoretically well-motivated, neither leads to strong predictability. The (effective) Yukawa coupling in the form of a 3×3 complex matrix introduces additional 18 real parametric degrees of freedom, and the space of parameters yielding the observed mass spectrum of quarks and leptons becomes enormously large. One may ask, in this large parameter space, which set of values is most likely realised in nature. For example, proximity to the original Georgi–Glashow $SU(5)$ model may be taken as a criterion for good parameter values. This is particularly the case for the 24-Higgs model involving a Planck-suppressed operator, which is naturally expected to be small. In [14], we used machine learning techniques for this purpose. Defining a loss function representing our criterion of naturalness as the closeness to the original Georgi–Glashow $SU(5)$ model, we demonstrated that the optimisation method of machine learning may be usefully applied to the problem where a brute-force parameter scan is not practical. With this criterion, it was found that the 24-Higgs model is statistically more natural than the 45-Higgs model.

The aim of the present paper is to extend the study of [14] in several directions. We first consider grand unification without supersymmetry. In [14] only the supersymmetric $SU(5)$ scenario was analysed, due mainly to its simplicity. Without convincing experimental data supporting supersymmetry thus far, it is reasonable to suppose that nature may well accomplish grand unification without supersymmetry. Our analysis shows that the result is, similar to the supersymmetric case, the 24-

* fayez@sokenengineering.com

† kawai@sci.kj.yamagata-u.ac.jp

‡ okadan@ua.edu

Higgs model is closer to the original model of Georgi and Glashow, and hence, is more natural than the 45-Higgs model. Another direction of extension is generalisation beyond the 24-Higgs or the 45-Higgs model. We develop a model parametrised by a continuous variable y that takes the value 3 for the 45-Higgs model and 1.5 for the 24-Higgs model. We find that the 24-Higgs model is not the most natural in this context; it turns out that the most natural case corresponds to $y \approx 0.8$.

In next section we review the $SU(5)$ GUT and lay out our notation of the flavour sector of the model. Sec. III presents results of the nonsupersymmetric $SU(5)$ GUT. Results of the supersymmetric case are given in Sec. IV, which partially overlap with the results of [14] but includes some technical improvements. The one-parameter generalised model is introduced and the results are presented in Sec. V. In Sec. VI we conclude with comments.

II. FERMION MASSES IN $SU(5)$ GUT

A. GUT mass relation of the minimal $SU(5)$ model

The $SU(5)$ Georgi-Glashow model [11] organises the quarks and leptons of the Standard Model into five and ten dimensional $SU(5)$ fermions $\Psi_{\mathbf{5}}^i$ and $\Psi_{\mathbf{10}}^i$, where $i \in \{1, 2, 3\}$ is the index for the family. For the first generation $i = 1$, the Standard Model fermions are embedded as

$$[\Psi_{\mathbf{5}}^1]^m = [d_1^c, d_2^c, d_3^c, e, -\nu_e], \quad (2)$$

$$[\Psi_{\mathbf{10}}^1]_{mn} = \frac{1}{\sqrt{2}} \begin{bmatrix} 0 & u_3^c & -u_2^c & -u_1 & -d_1 \\ -u_3^c & 0 & u_1^c & -u_2 & -d_2 \\ u_2^c & -u_1^c & 0 & -u_3 & -d_3 \\ u_1 & u_2 & u_3 & 0 & -e^c \\ d_1 & d_2 & d_3 & e^c & 0 \end{bmatrix}, \quad (3)$$

and similarly for $i = 2, 3$. The subscripts 1, 2, 3 for the u and d indicate the three colours of the quarks and $m, n, \dots \in \{1, 2, 3, 4, 5\}$ are the $SU(5)$ indices. We shall suppress the indices unless they are needed.

Besides the 3 families of fermionic fields $\Psi_{\mathbf{5}}^i$ and $\Psi_{\mathbf{10}}^i$, the $SU(5)$ model consists of a $\mathbf{24}$ representation gauge field, a $\mathbf{24}$ representation Higgs field $H_{\mathbf{24}}$ and a $\mathbf{5}$ representation Higgs field $H_{\mathbf{5}}$. The $H_{\mathbf{24}}$ field is responsible for GUT symmetry breaking $SU(5) \rightarrow SU(3)_c \times SU(2)_L \times U(1)_Y$, whereas the $H_{\mathbf{5}}$ field is responsible for the electroweak symmetry breaking $SU(2)_L \times U(1)_Y \rightarrow U(1)_{EM}$. The Yukawa part of the Lagrangian reads

$$y_{ij}^{5d} [\overline{\Psi_{\mathbf{5}}^i}]^m [\Psi_{\mathbf{10}}^j]_{mn} [H_{\mathbf{5}}]^n + y_{ij}^{5u} \epsilon^{mnpqr} [\overline{\Psi_{\mathbf{5}}^i}]_{mn} [\Psi_{\mathbf{10}}^j]_{pq} [H_{\mathbf{5}}]_r + \text{h.c.}, \quad (4)$$

where y_{ij}^{5u} , y_{ij}^{5d} are the Yukawa coupling matrices and ϵ is the antisymmetric tensor. Here in the nonsupersymmetric setup $H_{\mathbf{5}}$ is the complex conjugate of $H_{\mathbf{5}}$. Upon

electroweak symmetry breaking the $H_{\mathbf{5}}$ Higgs field is assumed to acquire vacuum expectation value

$$\langle [H_{\mathbf{5}}]_m \rangle = [0, 0, 0, 0, \frac{v_h}{\sqrt{2}}] \quad (5)$$

and the Lagrangian (4) becomes

$$y_{ij}^{5d} \frac{v_h}{\sqrt{2}} [\overline{\Psi_{\mathbf{5}}^i}]^m [\Psi_{\mathbf{10}}^j]_{m5} + y_{ij}^{5u} \frac{v_h}{\sqrt{2}} \epsilon^{mnpq5} [\overline{\Psi_{\mathbf{10}}^i}]_{mn} [\Psi_{\mathbf{10}}^j]_{pq} + \text{h.c.}, \quad (6)$$

from which the fermion mass matrices are found to be

$$M_u = 4 \frac{v_h}{\sqrt{2}} y_{ij}^{5u}, \quad M_d = \frac{v_h}{2} y_{ij}^{5d}, \quad M_e = \frac{v_h}{2} y_{ji}^{5d} = M_d^T. \quad (7)$$

The relations (1) follow from the last equation of (7). Using renormalisation group analysis, this prediction at the GUT scale may be compared with the low energy fermion masses that we know by experiments. It turns out that the third generation relation ($m_\tau = m_b$) is approximately consistent, but the relations for the first and second generations wildly violate the experimental constraints. This is the fermion mass problem, indicating that the model needs to be modified.

B. The 45-Higgs model

A well known solution [13] to the fermion mass problem is to include $\overline{\mathbf{45}}$ representation Higgs field¹ $H_{\overline{\mathbf{45}}}$ satisfying $[H_{\overline{\mathbf{45}}}]_m^{np} = -[H_{\overline{\mathbf{45}}}]_m^{pn}$, $[H_{\overline{\mathbf{45}}}]_m^{mp} = 0$, that has $SU(3)_c \times U(1)_Y$ -invariant vacuum expectation value

$$\langle [H_{\overline{\mathbf{45}}}]_m^{n5} \rangle = v_{45} \text{diag}(1, 1, 1, -3, 0). \quad (8)$$

An $SU(5)$ gauge invariant Yukawa term

$$y_{ij}^{45d} [\Psi_{\mathbf{5}}^i]^m [\Psi_{\mathbf{10}}^j]_{np} [H_{\overline{\mathbf{45}}}]_m^{np}, \quad (9)$$

with 3×3 complex Yukawa matrix y_{ij}^{45d} , then gives additional terms to the mass matrices. Including such contributions the mass matrices now read

$$\begin{aligned} M_u &= 2\sqrt{2} v_h y_{ij}^{5u}, \\ M_d &= \frac{v_h}{2} y_{ij}^{5d} + \frac{v_{45}}{\sqrt{2}} y_{ij}^{45d}, \\ M_e &= \frac{v_h}{2} y_{ji}^{5d} - 3 \frac{v_{45}}{\sqrt{2}} y_{ji}^{45d}. \end{aligned} \quad (10)$$

The fermion mass relations are seen to be modified by the new terms, and the observed fermion mass spectrum

¹ In the supersymmetric case (Sec. IV), this needs to be accompanied by the partner $H_{\mathbf{45}}$ in a vector-like pair $(\mathbf{45}, \overline{\mathbf{45}})$, which satisfies $[H_{\mathbf{45}}]_{np}^m = -[H_{\mathbf{45}}]_{pn}^m$, $[H_{\mathbf{45}}]_{mp}^m = 0$. A gauge invariant term $\epsilon^{mnpqr} [F_{\mathbf{10}}^i]_{mn} [F_{\mathbf{10}}^j]_{pq} [H_{\mathbf{45}}]_{rs}^q$ can arise, but it is not important for our discussions below.

at low energy can be recovered by adjusting y_{ij}^{5d} and y_{ij}^{45d} . For convenience let us write

$$M_5 \equiv \frac{v_h}{2} y_{ij}^{5d}, \quad M_{45} \equiv \frac{v_{45}}{\sqrt{2}} y_{ij}^{45d}. \quad (11)$$

Then the second and third lines of (10) are concisely

$$\begin{aligned} M_5 &= \frac{1}{4}(3M_d + M_e^T), \\ M_{45} &= \frac{1}{4}(M_d - M_e^T). \end{aligned} \quad (12)$$

C. The 24-Higgs model

An alternative solution to the fermion mass problem is to stay within the same field contents of the Georgi-Glashow model and take into account the effects of higher dimensional operator [12]

$$\frac{y_{ij}^{24d}}{m_P} [\bar{\Psi}_5^i]^m [H_{24}]_m^n [\Psi_{10}^j]_{np} [H_5]^p + \text{h.c.}, \quad (13)$$

which is a $SU(5)$ gauge singlet. Here, y_{ij}^{24d} is a new Yukawa-like coupling and m_P is the Planck mass. The H_{24} field acquires expectation value

$$H_{24} = v_{24} \text{diag}(2, 2, 2, -3, -3) \quad (14)$$

upon GUT symmetry breaking. The H_5 field acquires expectation value (5) below the electroweak scale, and here H_5 is the complex conjugate of H_5 . The fermion mass matrices including the effects from the higher dimensional term (13) then becomes,

$$\begin{aligned} M_u &= 2\sqrt{2}v_h y_{ij}^{5u}, \\ M_d &= \frac{v_h}{2} y_{ij}^{5d} + \frac{v_{24}}{m_P} v_h y_{ij}^{24d}, \\ M_e &= \frac{v_h}{2} y_{ji}^{5d} - \frac{3}{2} \frac{v_{24}}{m_P} v_h y_{ji}^{24d}. \end{aligned} \quad (15)$$

Tuning y_{ij}^{5d} and y_{ij}^{24d} the fermion mass spectrum observed at low energy is recovered via renormalisation group flow. Defining

$$M_{24} \equiv \frac{v_{24}}{2m_P} v_h y_{ij}^{24d}, \quad (16)$$

the last two lines of (15) are written

$$\begin{aligned} M_5 &= \frac{1}{5}(3M_d + 2M_e^T), \\ M_{24} &= \frac{1}{5}(M_d - M_e^T). \end{aligned} \quad (17)$$

D. Beauty of models and loss function

We often encounter situations in physics where a configuration predicted by a simple mathematical principle

(such as maximal symmetry) is not realised in nature, but instead experimental data exhibit slight deviations from it. The $SU(5)$ GUT under consideration clearly exemplifies this feature. In the parlance of [6, 14], the *point of beauty*, represented here by the Georgi-Glashow model, is at odds with the *truth*, namely the fermion mass spectrum observed in experiments. Our objective is to identify parameter values that optimally reconcile beauty with truth, that is, to locate a point in the parameter space as close as possible to the Georgi-Glashow model while remaining consistent with experimental constraints.

This conceptually straightforward task presents two technical challenges. The first concerns the size of the parameter space: due to its relatively high dimensionality, a brute-force scan is computationally infeasible. The central result of this paper, as we will demonstrate, is that this difficulty can be circumvented by employing machine learning techniques. The second challenge lies in defining the criterion of beauty, that is, quantifying the proximity to the Georgi-Glashow model within the parameter space. To address this, we examine the structure of the mass matrices that underlie the fermion mass problem. The Georgi-Glashow model predicts $M_d - M_e^T = 0$, corresponding to the third equation in (7), which is experimentally excluded. Indeed, as seen from (12) and (17), the modifications introduced via the 45-Higgs and 24-Higgs models are specifically designed to shift the value of $M_d - M_e^T$ away from zero. Our goal is to identify parameter values that are consistent with experimental data while remaining as close as possible to the point $M_d - M_e^T = 0$. To this end, we propose using $\det(M_d - M_e^T)$, appropriately normalised, as a measure of distance from the point of beauty. Note that the determinant is a convenient measure as it is invariant under unitary transformations. Specifically, as a dimensionless measure of this distance, we define

$$L = \left| \frac{\det(M_d - M_e^T)}{\det M_5} \right|, \quad (18)$$

and aim to minimise it subject to experimental constraints. The quantity (18) is regarded as a *loss function*. We shall use standard techniques of machine learning to optimise it in Secs.III, IV.

E. Parametrisation of the mass matrices

At energy scale $M_Z = 91.2$ GeV, the fermion masses are observed to be [15]

$$\begin{aligned}
m_u(M_Z) &= 0.00127, & m_c(M_Z) &= 0.634, & m_t(M_Z) &= 171, \\
m_d(M_Z) &= 0.00271, & m_s(M_Z) &= 0.0553, & m_b(M_Z) &= 2.86, \\
m_e(M_Z) &= 0.000487, & m_\mu(M_Z) &= 0.103, & m_\tau(M_Z) &= 1.75,
\end{aligned} \tag{19}$$

in GeV. The Cabibbo–Kobayashi–Maskawa (CKM) parameters are

$$s_{12}(M_Z) = 0.225, \quad s_{23}(M_Z) = 0.0411, \quad s_{13}(M_Z) = 0.00357, \quad \delta_{CP}(M_Z) = 1.24 \tag{20}$$

in the standard parametrisation (the form of the CKM matrix (27) below), and the strong CP phase is verified to be zero-consistent. We take into account these constraints and parametrise the Yukawa sector of the GUT, namely, separate the degrees of freedom that are observationally unconstrained.

Recall first that a 3×3 complex matrix can be diagonalised by two unitary matrices V and U . Then the up, down, and lepton Yukawa matrices are diagonalised as

$$\begin{aligned}
\frac{v_h}{\sqrt{2}} V_u^\dagger y^u U_u &= \text{diag}(m_u, m_c, m_t) \equiv D_u, \\
\frac{v_h}{\sqrt{2}} V_d^\dagger y^d U_d &= \text{diag}(m_d, m_s, m_b) \equiv D_d, \\
\frac{v_h}{\sqrt{2}} V_e^\dagger y^e U_e &= \text{diag}(m_e, m_\mu, m_\tau) \equiv D_e.
\end{aligned} \tag{21}$$

We will not discuss the neutrino Dirac Yukawa, assuming that the seesaw scale is not far from the GUT scale and hence the neutrino sector contributions are negligible. The CKM matrix is

$$V_{\text{CKM}} = V_u^\dagger V_d, \tag{22}$$

and the mass matrices M_u , M_d , M_e , appearing in (7), (10) and (15), are

$$\begin{aligned}
M_u &\equiv \frac{v_h}{\sqrt{2}} y^u = V_u D_u U_u^\dagger, \\
M_d &\equiv \frac{v_h}{\sqrt{2}} y^d = V_d D_d U_d^\dagger, \\
M_e &\equiv \frac{v_h}{\sqrt{2}} y^e = V_e D_e U_e^\dagger.
\end{aligned} \tag{23}$$

We choose the matrices V_u , U_u , V_e and U_e so that M_u and M_e are diagonal:

$$\begin{aligned}
M_u &= D_u = \text{diag}(m_u, m_c, m_t), \\
M_e &= D_e = \text{diag}(m_e, m_\mu, m_\tau).
\end{aligned} \tag{24}$$

This is always possible. Then M_d of (23) cannot be diagonalised. It is expressed, using $V_d = V_u V_{\text{CKM}}$ from (22), as

$$M_d = V_u V_{\text{CKM}} D_d U_d^\dagger, \tag{25}$$

where V_u is diagonal and U_d^\dagger is unitary. An arbitrary 3×3 unitary matrix has 9 real degrees of freedom and it

can be parametrised as

$$\begin{aligned}
U(\phi_0, \phi_1, \phi_2, \theta_1, \theta_2, \delta, \theta_3, \chi_1, \chi_2) \\
= e^{i\phi_0} e^{i(\phi_1 \lambda_3 + \phi_2 \lambda_8)} R(\theta_1, \theta_2, \delta, \theta_3) e^{i(\chi_1 \lambda_3 + \chi_2 \lambda_8)},
\end{aligned} \tag{26}$$

where $\lambda_3 = \text{diag}(1, -1, 0)$, $\lambda_8 = \text{diag}(1, 1, -2)/\sqrt{3}$ and

$$\begin{aligned}
R(\theta_1, \theta_2, \delta, \theta_3) \\
= \begin{pmatrix} 1 & 0 & 0 \\ 0 & c_1 & s_1 \\ 0 & -s_1 & c_1 \end{pmatrix} \begin{pmatrix} c_2 & 0 & s_2 e^{-i\delta} \\ 0 & 1 & 0 \\ -s_2 e^{i\delta} & 0 & c_2 \end{pmatrix} \begin{pmatrix} c_3 & s_3 & 0 \\ -s_3 & c_3 & 0 \\ 0 & 0 & 1 \end{pmatrix}
\end{aligned} \tag{27}$$

is a CKM-like matrix, with $s_i \equiv \sin \theta_i$ and $c_i \equiv \cos \theta_i$.

We are interested in the mass matrices M_u , M_d and M_e at the grand unification scale M_U . The diagonal ones are

$$\begin{aligned}
M_u(M_U) &= (m_u(M_U), m_c(M_U), m_t(M_U)), \\
M_e(M_U) &= (m_e(M_U), m_\mu(M_U), m_\tau(M_U)),
\end{aligned} \tag{28}$$

namely the fermion masses at the unification scale. In general, they differ from the low energy values (19) due to renormalisation group flow. Parametrising the unitary matrix U_d^\dagger as (26) and rearranging diagonal elements, the mass matrix (25) at the GUT scale is expressed using 11 real parameters x_0, \dots, x_{10} , $0 \leq x_i < 2\pi$, as

$$\begin{aligned}
M_d(M_U) \\
= e^{ix_0} e^{i(x_1 \lambda_3 + x_2 \lambda_8)} V_{\text{CKM}}(M_U) D_d(M_U) \\
\times e^{i(x_3 \lambda_3 + x_4 \lambda_8)} R(x_5, x_6, x_7, x_8) e^{i(x_9 \lambda_3 + x_{10} \lambda_8)},
\end{aligned} \tag{29}$$

where

$$D_d(M_U) = \text{diag}(m_d(M_U), m_s(M_U), m_b(M_U)). \tag{30}$$

These fermion masses and the CKM matrix $V_{\text{CKM}}(M_U)$ must be evaluated at the GUT scale M_U . They are obtained by solving renormalisation group equations, employing the low-energy values (19), (20) as boundary conditions. The renormalisation group flow is dependent on the scenario of GUT (supersymmetric or non-supersymmetric), as we elaborate on the details in the subsequent sections.

The bounds on the neutron electric dipole moment [16] indicates smallness of the strong CP parameter $|\bar{\theta}| \lesssim 10^{-10}$, which is related to the (topological) QCD angle θ_{QCD} and the fermion mass matrices as

$$\bar{\theta} = \theta_{\text{QCD}} - \arg \det(M_u M_d). \tag{31}$$

We assume the two terms of (31) separately vanish. As we chose M_u to be real and diagonal in (24), $\arg \det M_u$ is identically zero. Inspecting each factor of $M_d(M_U)$ in (29), it turns out that a nontrivial phase can arise only from the first factor. Then the condition for the vanishing CP angle

$$\arg \det(e^{ix_0} \mathbf{I}_{3 \times 3}) = \arg(e^{3ix_0}) = 0 \quad (32)$$

restricts x_0 to three possible values,

$$x_0 = 0, \quad \frac{2}{3}\pi, \quad \frac{4}{3}\pi. \quad (33)$$

Thus, considering the low energy data, we investigate the flavour sector of the $SU(5)$ model parametrised by 10 continuous variables $0 \leq x_i < 2\pi$, $i = 1, \dots, 10$ and three possible cases $x_0 = 0, \frac{2}{3}\pi, \frac{4}{3}\pi$.

III. NONSUPERSYMMETRIC SCENARIO

Apart from the observationally inconsistent prediction of the fermion mass relations (1), the Georgi-Glashow $SU(5)$ model presents three significant challenges: the three gauge coupling constants fail to unify at a single scale, the proton decay rate exceeds the experimental bounds, and substantial radiative corrections arise for light scalar particles (the hierarchy problem). It is widely acknowledged that these challenges are effectively addressed by supersymmetry; in the subsequent section, we will delve into the supersymmetric version of the $SU(5)$ model. In this section, our focus will be on the non-supersymmetric scenario, wherein at least the initial two aforementioned problems may be resolved through a minimally extended version of the original model.

A. $SU(5)$ GUT without supersymmetry

The Georgi-Glashow $SU(5)$ model below the GUT scale has the same matter contents as the Standard Model, and the three gauge coupling constants are known not to unify at one scale. In order to achieve unification without supersymmetry, we consider introducing four fermion fields as listed in Table I, in addition to the

TABLE I. Matter contents added to the Standard Model in the nonsupersymmetric $SU(5)$ GUT scenario. The representations in $SU(3)_c$, $SU(2)_L$, along with their corresponding $U(1)_Y$ charges and masses, are provided.

field	$SU(3)_c$	$SU(2)_L$	$U(1)_Y$	mass
d'	3	1	$\frac{1}{6}$	$\left. \vphantom{\begin{matrix} d' \\ \bar{d}' \end{matrix}} \right\} m_D = 4.6 \times 10^8 \text{ GeV}$
\bar{d}'	3*	1	$-\frac{1}{6}$	
q'	3	2	$-\frac{1}{3}$	$\left. \vphantom{\begin{matrix} q' \\ \bar{q}' \end{matrix}} \right\} m_Q = 2 \text{ TeV}$
\bar{q}'	3*	2	$\frac{1}{3}$	

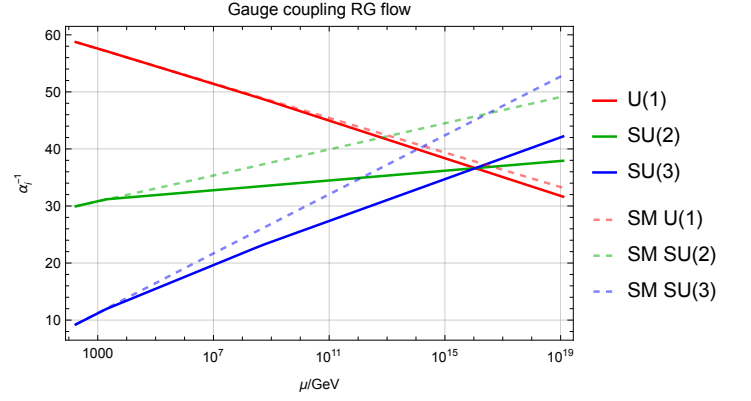


FIG. 1. Renormalisation group flow of $\alpha_i^{-1} \equiv 4\pi/g_i^2$, for the three gauge coupling constants g_1, g_2, g_3 . The solid lines are the solution for the $m_D = 4.6 \times 10^8 \text{ GeV}$ and $m_Q = 2 \text{ TeV}$ case. The dashed lines represent the gauge couplings of the Standard Model.

matter contents of the Standard Model (namely those of the original $SU(5)$ model below the GUT scale). The fields d', \bar{d}' , having the Dirac mass m_D , form a vectorlike pair and leave the anomaly cancellation intact. They are split multiplets included in vectorlike $SU(5)$ fermions $\mathbf{5} + \bar{\mathbf{5}}$ [17, 18]. Likewise, q' and \bar{q}' are split multiplets arising from a vectorlike pair $\mathbf{10} + \bar{\mathbf{10}}$. Thus we consider an $SU(5)$ GUT model with extra $\mathbf{5} + \bar{\mathbf{5}}$ and $\mathbf{10} + \bar{\mathbf{10}}$ multiplets added to the Georgi-Glashow model.

The running of the gauge coupling constants, g_3 of $SU(3)_c$, g_2 of $SU(2)_L$ and $g_1 = \sqrt{5/3}g_Y$ of $U(1)_Y$ is modified by the vectorlike fermions. The renormalisation group equations for the gauge couplings are (at one-loop) $dg_i/d \ln \mu = g_i^3 b_i / 16\pi^2$, with beta functions

$$b_i = (b_1, b_2, b_3) = b_i^{\text{SM}} + \Delta b_i^Q + \Delta b_i^D, \quad (34)$$

$$b_i^{\text{SM}} = \left(\frac{41}{10}, -\frac{19}{6}, -7 \right),$$

$$\Delta b_i^Q = \left(\frac{2}{15}, 2, \frac{4}{3} \right) \text{ for } \mu > m_Q, \text{ 0 otherwise,}$$

$$\Delta b_i^D = \left(\frac{4}{15}, 0, \frac{2}{3} \right) \text{ for } \mu > m_D, \text{ 0 otherwise.}$$

When the vectorlike fermions have masses $m_D = 4.6 \times 10^8 \text{ GeV}$ and $m_Q = 2 \text{ TeV}$, as listed in Table I, the three gauge couplings are found to unify² at $M_U = 1.13 \times 10^{16} \text{ GeV}$. Fig. 1 shows the flow of the gauge couplings in this case. This unification scale is sufficiently high so that this scenario is consistent with the present proton decay bounds [20, 21]. We use this as our benchmark scenario of nonsupersymmetric $SU(5)$ GUT.

The Yukawa couplings at the GUT scale are determined by the fermion masses at low energies through the

² We used boundary conditions of [19].

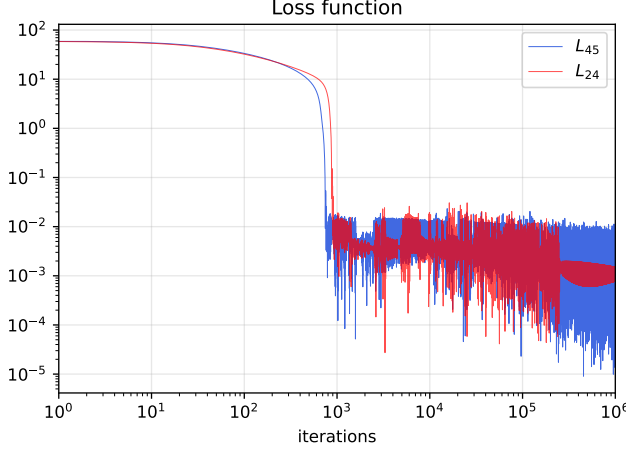


FIG. 2. A sample of the loss function evolution for the 45-Higgs model (blue) and the 24-Higgs model (red), in the non-supersymmetric scenario of Table I. We selected $x_0 = 0$ and employed the identical set of 10 initial parameters for both the 45-Higgs model and the 24-Higgs model. We utilised the Adam algorithm [22] for optimisation and conducted iteration up to $N_{\text{iter}} = 10^6$ steps.

renormalisation group equations. Denoting the Yukawa matrices collectively as y^f , $f = \{u, d, e\}$ and introducing $S_f \equiv (y^f)^\dagger y^f$ for convenience, the renormalisation group equations for the Yukawa couplings are written

$$16\pi^2 \frac{dS_f}{d\ln\mu} = \beta_f S_f + S_f \beta_f, \quad (35)$$

$$\begin{aligned} m_u(M_U) &= 0.000496, & m_c(M_U) &= 0.247, & m_t(M_U) &= 75.9, \\ m_d(M_U) &= 0.00109, & m_s(M_U) &= 0.0223, & m_b(M_U) &= 1.01, \\ m_e(M_U) &= 0.000470, & m_\mu(M_U) &= 0.0995, & m_\tau(M_U) &= 1.69, \end{aligned} \quad (38)$$

in GeV and the CKM matrix parameters

$$s_{12}(M_U) = 0.225, \quad s_{23}(M_U) = 0.0467, \quad s_{13}(M_U) = 0.00406, \quad \delta_{CP}(M_U) = 1.24. \quad (39)$$

We use these values in the following numerical analysis as input data for the nonsupersymmetric GUT scenario.

³ These values are derived by integrating the equations from the top pole mass, $M_t = 173.34$ GeV, while employing the low-energy data at M_Z instead of M_t , which serves as a suitable approximation.

with beta functions

$$\begin{aligned} \beta_u &= \frac{3}{2}S_u - \frac{3}{2}S_d \\ &+ \left\{ 3 \text{Tr } S_u + 3 \text{Tr } S_d + \text{Tr } S_e - \frac{17}{20}g_1^2 - \frac{9}{4}g_2^2 - 8g_3^2 \right\} \mathbb{1}, \\ \beta_d &= \frac{3}{2}S_d - \frac{3}{2}S_u \\ &+ \left\{ 3 \text{Tr } S_u + 3 \text{Tr } S_d + \text{Tr } S_e - \frac{1}{4}g_1^2 - \frac{9}{4}g_2^2 - 8g_3^2 \right\} \mathbb{1}, \\ \beta_e &= \frac{3}{2}S_e + \left\{ 3 \text{Tr } S_u + 3 \text{Tr } S_d + \text{Tr } S_e - \frac{9}{4}g_1^2 - \frac{9}{4}g_2^2 \right\} \mathbb{1}. \end{aligned} \quad (36)$$

Here $\mathbb{1}$ is the 3×3 unit matrix. The boundary conditions at the low energy are given by

$$\begin{aligned} S_u &= \text{diag} \left(\frac{2m_u^2}{v_h^2}, \frac{2m_c^2}{v_h^2}, \frac{2m_t^2}{v_h^2} \right), \\ S_d &= V_{\text{CKM}} \text{diag} \left(\frac{2m_d^2}{v_h^2}, \frac{2m_s^2}{v_h^2}, \frac{2m_b^2}{v_h^2} \right) V_{\text{CKM}}^\dagger, \\ S_e &= \text{diag} \left(\frac{2m_e^2}{v_h^2}, \frac{2m_\mu^2}{v_h^2}, \frac{2m_\tau^2}{v_h^2} \right), \end{aligned} \quad (37)$$

where $v_h = 246$ GeV. The fermion masses and the CKM matrix at $\mu = M_Z$ are those given by (19).

The Yukawa couplings (in the form of the eigenvalues of the mass matrices) and the CKM matrix at unification scale $\mu = M_U$ are found by integrating (35) up to the unification scale³. We find the fermion masses

B. Good parameter values: numerical method

Under the assumption of this particular grand unification scenario, the fermion mass parameters and the CKM matrix at the GUT scale are determined as specified in (38) and (39). The remaining unfixed parameters of the model are x_0, \dots, x_{10} , as defined in equation (29). Among these parameters, x_0 can assume one of the three discrete values: 0, $2\pi/3$, or $4\pi/3$, due to the constraints imposed by the vanishing strong CP phase. The remaining parameters, x_1, \dots, x_{10} , are phase parameters and can take continuous values within the range $0 \leq x_i < 2\pi$.

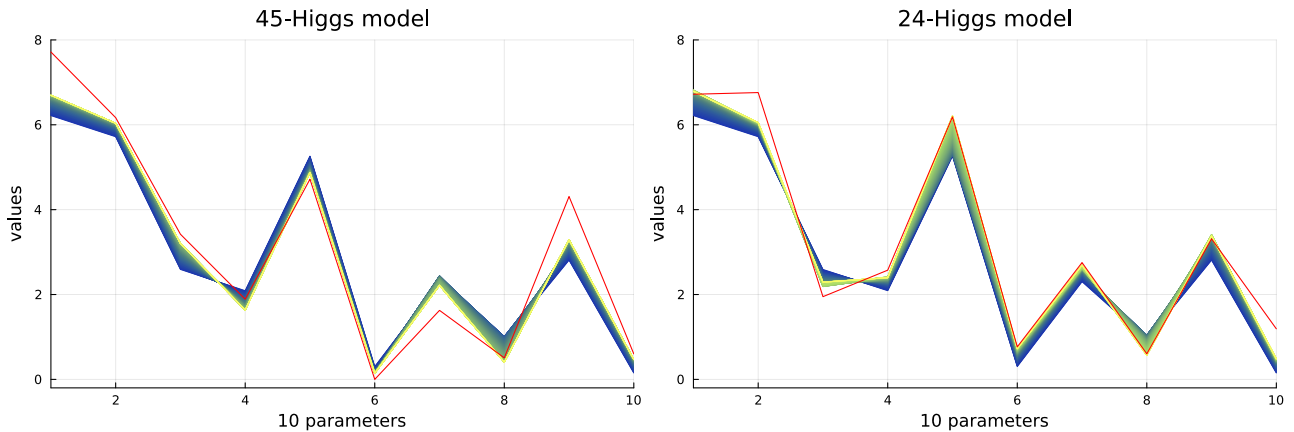


FIG. 3. Evolution of the ten parameters, x_i , $i = 1, 2, \dots, 10$, in the same sample of optimisation processes shown in Fig. 2, for the 45-Higgs model (left panel) and the 24-Higgs model (right). The darkest blue represents the initial random values of the parameters ($N_{\text{iter}} = 0$), which are chosen to be identical for the two models. The brightest yellow represents the parameter configuration at $N_{\text{iter}} = 1,000$, with an interval of 10 steps in between. The red lines represent the configurations after $N_{\text{iter}} = 10^6$ steps. The parameters of the two models begin with the same initial configurations and are observed to be adjusted to distinct optimised values.

The objective of our analysis is to identify within the parameter space the distribution of parameter values that are deemed to be natural. For the 45-Higgs and 24-Higgs models, and for each of the discrete parameter values of x_0 , we carry out the analysis following three steps:

Sampling: Generate initial values of the ten parameters x_1, \dots, x_{10} by randomly sampling from the uniform distribution $0 \leq x_i < 2\pi$.

Optimisation: Starting with the initial values, minimise the loss function (18) using an optimisation scheme of machine learning.

Statistics: Repeat sampling and optimisation N_{samp} times and analyse the optimised loss function and the parameter values of the collected samples.

For numerical optimisation, we employ the vanilla Adam algorithm [22] with hyperparameters $\alpha = 0.001$, $\beta_1 = 0.9$, $\beta_2 = 0.999$, and $\epsilon = 10^{-8}$. An example of optimisation process, with a single initial set of parameters, is presented in Figs. 2 and 3. In this example, the discrete parameter is chosen to be $x_0 = 0$, and iteration is taken $N_{\text{iter}} = 10^6$ steps. Fig. 2 depicts the evolution of the loss function (18), with the blue curve representing the 45-Higgs model and the red curve representing the 24-Higgs model. Fig. 3 illustrates the evolution of the 10 parameter values during optimisation. The 45-Higgs model (left) and the 24-Higgs model (right) commence with the same initial configuration (dark blue), but they are observed to converge to distinct optimised states (indicated by red lines). Furthermore, this example demonstrates that the excursion of the parameter values is relatively small ($\lesssim 1$), suggesting that the loss function possesses numerous local minima. Consequently, it is imperative to commence with a multitude of distinct initial configurations

in order to explore the parameter space of the model.

C. 45-Higgs model vs. 24-Higgs model

We collected 1024 samples of numerical optimisation with randomly chosen initial configurations, each for the 45-Higgs and 24-Higgs models and for the discrete parameter values $x_0 = 0, 2\pi/3$ and $4\pi/3$. The distribution of the 1024 minimised values of the loss function, defined in (18), for each case is shown in Fig. 4. Here, we evaluated the minimised loss function value by averaging over the final 100 steps (i.e. 999,901st-1,000,000th) of the total $N_{\text{iter}} = 10^6$ iterations, in order to mitigate the effects of fluctuations (see Fig. 2). In all three cases of $x_0 = 0, 2\pi/3$ and $4\pi/3$, the loss function of the 24-Higgs model, depicted in red, is seen to be distributed at smaller values than that of the 45-Higgs model (blue). This indicates the tendency that the 24-Higgs model lies closer to the original Georgi-Glashow model than the 45-Higgs model does. Thus, according to our definition of naturalness, the 24-Higgs model is more natural than the 45-Higgs model.

As illustrated in Fig. 3, the parameters x_1, \dots, x_{10} are adjusted to their optimal values, as indicated by the red lines, to minimise the loss function. Fig. 5 presents the optimised configurations of parameters x_1, \dots, x_{10} for the 45-Higgs and 24-Higgs models, for values of $x_0 = 0, 2\pi/3$ and $4\pi/3$. Each panel displays only 100 samples out of 1024, representing the 100 smallest values of the minimised loss function. Darker (lighter) blue colours correspond to smaller (larger) loss function values. A smaller loss function indicates a more natural parameter configuration. Consequently, regions in darker blue indicate preferred parameter values, while blank regions are dis-

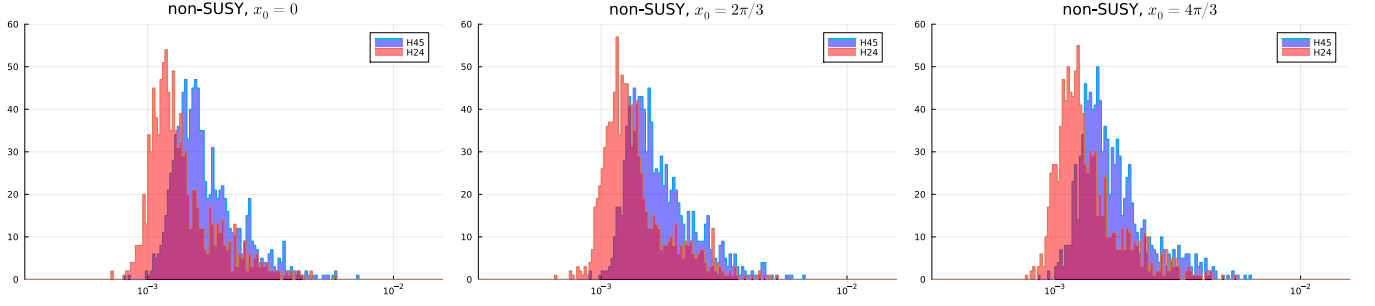


FIG. 4. Distribution of optimised loss function values for $N_{\text{samp}} = 1024$ samples, in the nonsupersymmetric $SU(5)$ GUT scenario. The left, middle, and right panels present the results for $x_0 = 0$, $2\pi/3$, and $4\pi/3$, respectively. The 45-Higgs model (H45) is depicted in blue, while the 24-Higgs model (H24) is shown in red. An optimised value is determined by averaging over the final 100 steps of the total $N_{\text{iter}} = 10^6$ iterations, thereby mitigating the influence of fluctuations (refer to Fig. 2). In all three cases, the loss function of the 24-Higgs model exhibits a distribution of smaller values compared to that of the 45-Higgs model.

favoured.

The three values of x_0 all give similar results. Thus our criterion of naturalness does not favour or disfavour a particular value of x_0 that avoids the strong CP problem.

IV. SUPERSYMMETRIC SCENARIO

A. Supersymmetric $SU(5)$ GUT

The supersymmetric version of the minimal $SU(5)$ GUT consists of a $\mathbf{24}$ representation vector multiplet $V_{\mathbf{24}}$, one $\mathbf{24}$, one $\mathbf{5}$, one $\bar{\mathbf{5}}$ and three copies of $\mathbf{10}$ and $\bar{\mathbf{5}}$ representation chiral multiplets of $SU(5)$ that we denote by $H_{\mathbf{24}}$, $H_{\mathbf{5}}$, $H_{\bar{\mathbf{5}}}$, $F_{\mathbf{10}}^i$ and $F_{\bar{\mathbf{5}}}^i$ respectively. The $SU(5)$ fermions $\Psi_{\bar{\mathbf{5}}}^i$ of Eq. (2) and $\Psi_{\mathbf{10}}^i$ of Eq. (3) are the fermionic parts of $F_{\bar{\mathbf{5}}}^i$ and $F_{\mathbf{10}}^i$. The bosonic parts of the chiral multiplets $H_{\mathbf{24}}$ and $H_{\mathbf{5}}$ are the $\mathbf{24}$ and $\mathbf{5}$ representation Higgs fields represented by the same symbols. While $H_{\bar{\mathbf{5}}}$ in (4) was the complex conjugate of $H_{\mathbf{5}}$ in the nonsupersymmetric scenario, here $H_{\bar{\mathbf{5}}}$ is (the bosonic part of) a separate chiral supermultiplet. Consequently the $\mathbf{5}$ and $\bar{\mathbf{5}}$ Higgs may acquire distinct vacuum expectation values

$$\langle H_{\mathbf{5}} \rangle = [0, 0, 0, 0, \frac{v_u}{\sqrt{2}}], \quad \langle H_{\bar{\mathbf{5}}} \rangle = [0, 0, 0, 0, \frac{v_d}{\sqrt{2}}]. \quad (40)$$

We assume their ratio to be fixed, $\tan\beta \equiv v_d/v_u = 10$, in the numerics. The superpotential of the minimal supersymmetric $SU(5)$ model is given by

$$\begin{aligned} W_{\text{min}} = & \frac{m_{\Sigma}}{2} \text{Tr}(H_{\mathbf{24}})^2 + \frac{\lambda_{\Sigma}}{3} \text{Tr}(H_{\mathbf{24}})^3 \\ & + H_{\bar{\mathbf{5}}} (m_H + \lambda_H H_{\mathbf{24}}) H_{\mathbf{5}} \\ & - y_{ij}^{5d} [F_{\bar{\mathbf{5}}}^i]^m [F_{\mathbf{10}}^j]_{mn} [H_{\mathbf{5}}]^n \\ & - y_{ij}^{5u} \epsilon^{mnpqr} [F_{\mathbf{10}}^i]_{mn} [F_{\mathbf{10}}^j]_{pq} [H_{\bar{\mathbf{5}}}]_r, \end{aligned} \quad (41)$$

where m_{Σ} , λ_{Σ} , m_H and λ_H are real parameters. The Yukawa part of the Lagrangian is

$$\begin{aligned} y_{ij}^{5d} \frac{v_d}{\sqrt{2}} [\bar{\Psi}_{\bar{\mathbf{5}}}^i]^m [\Psi_{\mathbf{10}}^j]_{m5} + y_{ij}^{5u} \frac{v_u}{\sqrt{2}} \epsilon^{mnpq5} [\bar{\Psi}_{\mathbf{10}}^i]_{mn} [\Psi_{\mathbf{10}}^j]_{pq} \\ + \text{h.c.}, \end{aligned} \quad (42)$$

and the mass matrices are

$$M_u = 4 \frac{v_u}{\sqrt{2}} y_{ij}^{5u}, \quad M_d = \frac{v_d}{2} y_{ij}^{5d}, \quad M_e = \frac{v_d}{2} y_{ji}^{5d} = M_d^T, \quad (43)$$

leading to the same GUT mass relations (1).

The supersymmetric version of the 45-Higgs model posits the presence of an additional chiral superfield, denoted as $H_{\mathbf{45}}$, along with its corresponding superpotential

$$W_{\mathbf{45}} = y_{ij}^{45d} [F_{\bar{\mathbf{5}}}^i]^m [F_{\mathbf{10}}^j]_{np} [H_{\mathbf{45}}]_m^{np}. \quad (44)$$

Assuming the vacuum expectation value (8), the mass matrices are modified from (43) as

$$\begin{aligned} M_u = & 2\sqrt{2} v_u y_{ij}^{5u}, \\ M_d = & \frac{v_d}{2} y_{ij}^{5d} + \frac{v_{45}}{\sqrt{2}} y_{ij}^{45d}, \\ M_e = & \frac{v_d}{2} y_{ji}^{5d} - 3 \frac{v_{45}}{\sqrt{2}} y_{ji}^{45d}. \end{aligned} \quad (45)$$

The alternative, 24-Higgs approach incorporates contributions from a higher dimensional $SU(5)$ gauge singlet term $F_{\bar{\mathbf{5}}} H_{\mathbf{24}} F_{\mathbf{10}} H_{\bar{\mathbf{5}}} \subset W$ which gives rise to the term in the Lagrangian (13). The GUT Higgs field $H_{\mathbf{24}}$ acquires a vacuum expectation value $H_{\mathbf{24}} = (m_{\Sigma}/\lambda_{\Sigma}) \text{diag}(2, 2, 2, -3, -3)$. The expectation value of $H_{\bar{\mathbf{5}}}$ is specified by (40). Then the fermion mass matrices

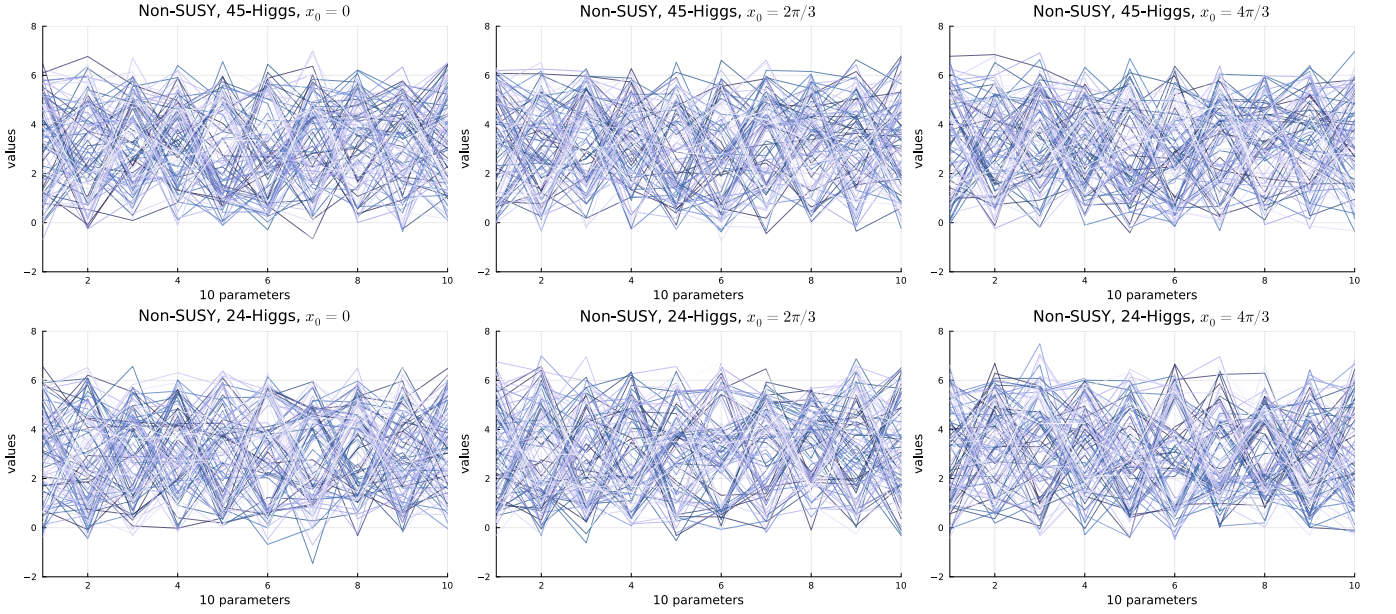


FIG. 5. Optimised configurations of ten parameters x_1, \dots, x_{10} in the nonsupersymmetric $SU(5)$ GUT scenario. The upper (lower) panels present the results for the 45-Higgs (24-Higgs) model. The cases where $x_0 = 0, 2\pi/3$, and $4\pi/3$ are depicted on the left, middle, and right panels, respectively. Each panel displays 100 samples representing the 100 smallest values of the loss function out of the 1024 available samples. Darker lines correspond to the smaller loss function values.

in this case become

$$\begin{aligned} M_u &= 2\sqrt{2}v_u y_{ij}^{5u}, \\ M_d &= \frac{v_d}{2} y_{ij}^{5d} + \frac{m_\Sigma}{m_P \lambda_\Sigma} v_d y_{ij}^{24d}, \\ M_e &= \frac{v_d}{2} y_{ji}^{5d} - \frac{3}{2} \frac{m_\Sigma}{m_P \lambda_\Sigma} v_d y_{ji}^{24d}. \end{aligned} \quad (46)$$

Thus the formulation of the fermion mass matrices parallels the nonsupersymmetric case. Introducing

$$\begin{aligned} M_5 &\equiv \frac{v_d}{2} y_{ij}^{5d}, \quad M_{45} \equiv \frac{v_{45}}{\sqrt{2}} y_{ij}^{45d}, \\ M_{24} &\equiv \frac{m_\Sigma}{2m_P \lambda_\Sigma} v_d y_{ij}^{24d}, \end{aligned} \quad (47)$$

the modified GUT mass relations of the 45-Higgs model (45) and the 24-Higgs model (46) are written in the same forms as the nonsupersymmetric scenario, (12) and (17).

Assuming low supersymmetry breaking scale $M_S \simeq 10$ TeV, we use the renormalisation group equations of the MSSM from $\mu = M_Z = 91.2$ GeV⁴. At one loop, the beta functions for the gauge couplings are $b_i \equiv (b_1, b_2, b_3) = (33/5, 1, -3)$ and the GUT scale is $M_U \simeq 3 \times 10^{16}$ GeV. The renormalisation group equations for the Yukawa cou-

plings (4) now have beta functions [24]

$$\begin{aligned} \beta_u &= 3S_u + S_d + \left\{ \text{Tr}(3S_u) - \frac{13}{15}g_1^2 - 3g_2^2 - \frac{16}{3}g_3^2 \right\} \mathbb{1}, \\ \beta_d &= 3S_d + S_u + \left\{ \text{Tr}(3S_d + S_e) - \frac{7}{15}g_1^2 - 3g_2^2 - \frac{16}{3}g_3^2 \right\} \mathbb{1}, \\ \beta_e &= 3S_e + \left\{ \text{Tr}(3S_d + S_e) - \frac{9}{5}g_1^2 - 3g_2^2 \right\} \mathbb{1}. \end{aligned} \quad (48)$$

The boundary conditions for the Yukawa couplings at $\mu = M_Z$ are set as

$$\begin{aligned} S_u &= \text{diag} \left(\frac{m_u^2}{v^2}, \frac{m_c^2}{v^2}, \frac{m_t^2}{v^2} \right) \left(1 + \frac{1}{\tan^2 \beta} \right), \\ S_d &= V_{\text{CKM}} \text{diag} \left(\frac{m_d^2}{v^2}, \frac{m_s^2}{v^2}, \frac{m_b^2}{v^2} \right) V_{\text{CKM}}^\dagger (1 + \tan^2 \beta), \\ S_e &= \text{diag} \left(\frac{m_e^2}{v^2}, \frac{m_\mu^2}{v^2}, \frac{m_\tau^2}{v^2} \right) \left(1 + \frac{1}{\tan \beta} \right), \end{aligned} \quad (49)$$

in the basis where S_u and S_e are diagonal. The fermion mass parameters at the GUT scale $\mu = M_U$ are found to be

⁴ This approximation is consistent in the parameter region where the Super-Kamiokande bounds [23] on the proton decay through

the 5-dimensional operator are satisfied.

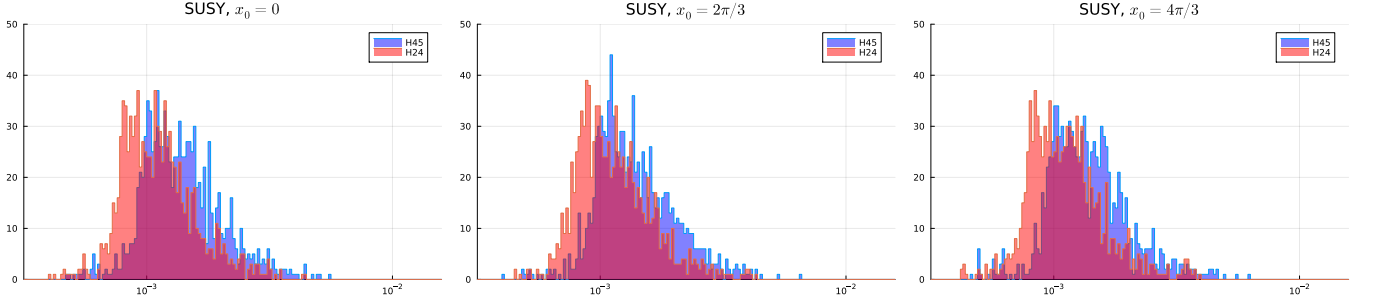


FIG. 6. Distribution of optimised loss function values for $N_{\text{samp}} = 1024$ samples, in the supersymmetric $SU(5)$ GUT scenario. The left, middle, and right panels present the results for $x_0 = 0$, $2\pi/3$, and $4\pi/3$, respectively. The 45-Higgs model (H45) is depicted in blue, while the 24-Higgs model (H24) is shown in red. An optimised value is determined by averaging over the final 100 steps of the total $N_{\text{iter}} = 10^6$ iterations, thereby mitigating the influence of fluctuations (refer to Fig. 2). In all three cases, the loss function of the 24-Higgs model exhibits a distribution of smaller values compared to that of the 45-Higgs model.

$$\begin{aligned}
 m_u(M_U) &= 0.000502, & m_c(M_U) &= 0.251, & m_t(M_U) &= 97.7, \\
 m_d(M_U) &= 0.000769, & m_s(M_U) &= 0.0157, & m_b(M_U) &= 0.922, \\
 m_e(M_U) &= 0.000324, & m_\mu(M_U) &= 0.0685, & m_\tau(M_U) &= 1.17,
 \end{aligned} \tag{50}$$

in GeV. The CKM matrix parameters are

$$s_{12}(M_U) = 0.225, \quad s_{23}(M_U) = 0.0363, \quad s_{13}(M_U) = 0.00315, \quad \delta_{CP}(M_U) = 1.24. \tag{51}$$

B. Good parameter values: numerical method

Our purpose is to investigate the parameter space of the flavour sector using the methods of machine learning, namely, sampling, optimisation and statistical analysis as described in Sec. IIIB. Here we study the 45-Higgs model and 24-Higgs model of the supersymmetric $SU(5)$. We use the same criterion of naturalness specified by the loss function (18). The mass matrices in the supersymmetric $SU(5)$ scenario are in the same forms as the nonsupersymmetric case, (12) and (17). The structure of the Higgs sector is different in that there are two Higgs quintets in the supersymmetric scenario that can take different expectation values v_u and $v_d = v_u \tan \beta$. However, the fermion mass relations are concerned only with v_d , and the difference of v_u and v_d is absorbed by rescaling y^{5u} . Thus in practice, the difference between the supersymmetric and nonsupersymmetric scenarios is only in the renormalisation group equations. Hence, we shall use the fermion mass data at the unification scale, (50) and (51), and repeat the numerical studies explained in Sec. III.

C. 45-Higgs model vs. 24-Higgs model

We optimised the 10 parameters x_1, \dots, x_{10} for both 45-Higgs and 24-Higgs models, with the discrete param-

eter value of x_0 chosen to be 0, $2\pi/3$ and $4\pi/3$. The loss function⁵ to be minimised is (18), where M_d , M_e^T and M_5 are given by (12) for the 45-Higgs model and (17) for the 24-Higgs model.

In each case, we collected 1024 numerical samples (i.e., $2 \times 3 = 6$ sets). Fig. 6 illustrates the distribution of the minimised values of the loss function. We conducted optimisation with $N_{\text{iter}} = 10^6$ iteration steps, and the minimised loss function values were obtained by averaging over the last 100 steps. It is observed that for all cases of $x_0 = 0$, $2\pi/3$, and $4\pi/3$, the minimised values of the loss function for the 24-Higgs model are distributed at smaller values compared to those of the 45-Higgs model. This suggests that the 24-Higgs model is more natural, or more beautiful [6], than the 45-Higgs model. The results of the three cases, $x_0 = 0$, $2\pi/3$, $4\pi/3$, are observed to be similar and these three values of x_0 are deemed equally natural.

Fig. 7 illustrates the optimised configurations of the ten parameters x_1, \dots, x_{10} that minimise the loss function after $N_{\text{iter}} = 10^6$ iteration steps. Each panel displays samples representing the top 100 out of 1024, which cor-

⁵ The definition of the loss function (18) differs from the one used in [14] by normalisation. We use (18) here as it is more convenient when the generalised model of Sec. V is discussed. So far as the 45-Higgs and 24-Higgs model are concerned this redefinition does not alter the conclusion of Ref. [14].

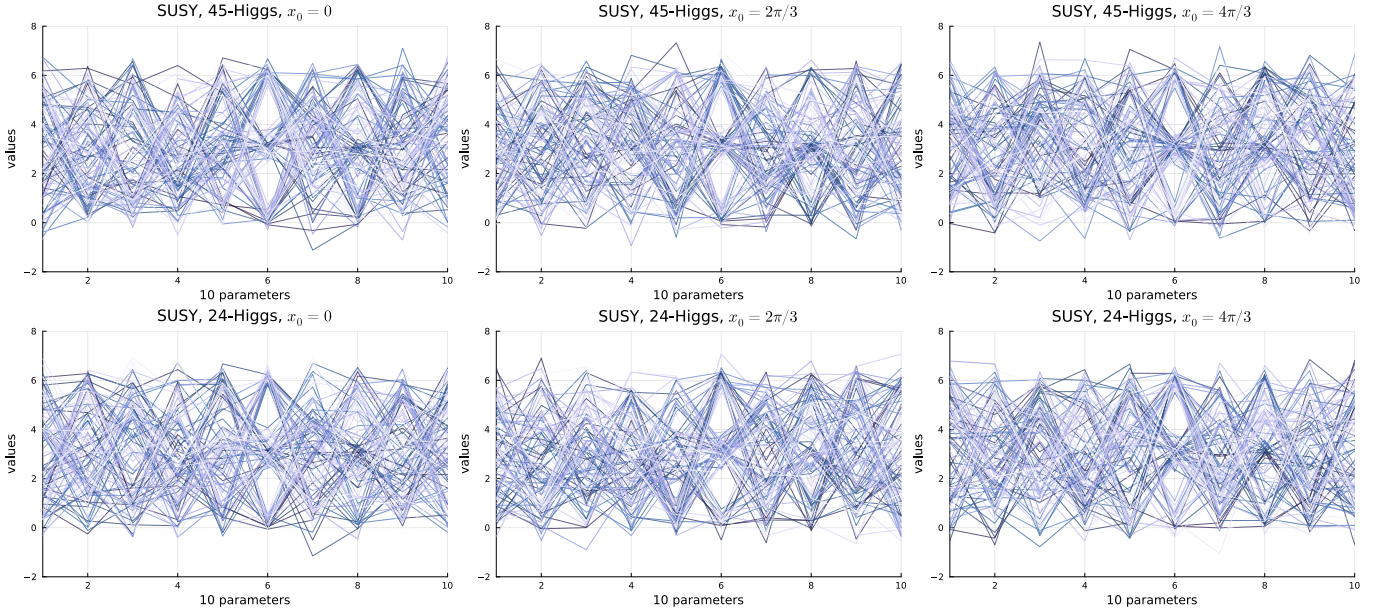


FIG. 7. Optimised configurations of ten parameters x_1, \dots, x_{10} in the supersymmetric $SU(5)$ GUT scenario. The upper (lower) panels present the results for the 45-Higgs (24-Higgs) model. The cases where $x_0 = 0, 2\pi/3$, and $4\pi/3$ are depicted on the left, middle, and right panels, respectively. Each panel displays 100 samples representing the 100 smallest values of the loss function out of the 1024 available samples. Darker lines correspond to the smaller loss function values.

respond to the smallest minimised loss function values. Darker blue indicates a smaller value of the minimised loss function, thereby representing the favoured parameter configurations according to our criteria of naturalness.

V. ONE-PARAMETER GENERALISATION

A. Generalisation of 45-Higgs and 24-Higgs models

The original $SU(5)$ GUT proposed by Georgi and Glashow [11] presents an elegant framework, although it is in conflict with the observed fermion masses. We discussed above the two notable improved models: the 45 Higgs model by Georgi and Jarlskog [13] and the 24 Higgs model by Ellis and Gaillard [12]. These improved models, while successfully accommodate the observed fermion mass spectrum, involve numerous additional degrees of freedom that compromise their predictability. In the preceding sections, we examined these models, both for non-supersymmetric and supersymmetric scenarios, and discovered that the 24-Higgs model exhibits a more proximity to the original Georgi-Glashow model, as determined by the criteria of proximity defined in terms of the loss function. In this section we pose another question, whether there exists a model that can approach closer to the Georgi-Glashow model than the 24-Higgs model. Machine learning techniques are found to be useful for this problem.

We saw that the mass matrices in the 45 Higgs were

$$M_d = M_5 + M_{45}, \quad M_e^T = M_5 - 3M_{45}, \quad (52)$$

and those of the 24 Higgs model were

$$M_d = M_5 + 2M_{24}, \quad M_e^T = M_5 - 3M_{24}. \quad (53)$$

These are in the form of

$$M_d = M_5 + aM, \quad M_e^T = M_5 - bM, \quad (54)$$

if the matrices M_{45} and M_{24} are denoted by M . Two parameters a and b are assumed to be real and positive. The 45-Higgs model is realised by $(a, b) = (1, 3)$, and the 24-Higgs model is realised by $(a, b) = (2, 3)$, as special cases of this generalised model.

We consider the same loss function (18). Using (54), it can be written

$$\begin{aligned} L &= \left| \frac{\det(M_d - M_e^T)}{\det(M_5)} \right| \\ &= (a+b)^3 \left| \frac{\det(M_d - M_e^T)}{\det(bM_d + aM_e^T)} \right| \\ &= (1+y)^3 \left| \frac{\det(M_d - M_e^T)}{\det(yM_d + M_e^T)} \right|, \end{aligned} \quad (55)$$

where $y = b/a$ is a real, continuous parameter. Given that a and b were both assumed to be positive, $y = b/a$ must also be positive. The generalised model represents the 45-Higgs model when $y = 3$ and the 24-Higgs model when $y = 1.5$. To justify this model, one may consider, for instance, a situation where the $\overline{45}$ representation Higgs and the higher-dimensional operator may coexist, and both (9) and (13) may contribute to the Lagrangian of the model. If the Yukawa matrices of these

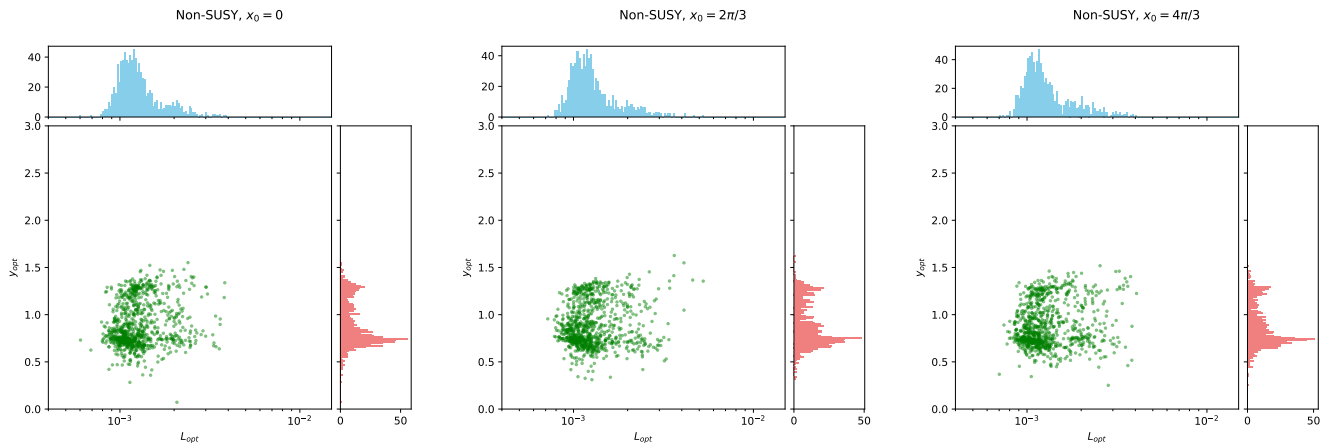


FIG. 8. Optimised values of the loss function and parameter y , for $x_0 = 0$ (left panel), $x_0 = 2\pi/3$ (middle) and $x_0 = 4\pi/3$ (right), in the generalised model of nonsupersymmetric $SU(5)$ GUT. Optimisation was conducted for iteration steps $N_{\text{iter}} = 10^6$ and 1024 samples were collected for each case. A small fraction ($< 10\%$) of samples resulted in $y < 0$ and were discarded. The optimised (minimised) loss function values are the average of the last 100 steps. The distribution of the optimised values for the loss function (light blue) and y (pink) are also presented in subplots.

two terms are proportional, the model reduces to our case.

Our standard of naturalness, or the *beauty*, is the same as before. We minimise the loss function (55), by optimising eleven parameters, x_1, \dots, x_{10} and y . Our aim here is to find the optimal value of y by machine learning.

B. Nonsupersymmetric scenario

In this subsection, we consider the nonsupersymmetric scenario. Similar to the analysis presented in Sec. III, we examine the nonsupersymmetric $SU(5)$ model depicted in Table I and utilise the fermion mass data provided in Eqs. (38) and (39) at the unification scale. We investigate three distinct cases, each with a different value for x_0 : $x_0 = 0$, $2\pi/3$, and $4\pi/3$. To begin, we generate randomly initialised data consisting of eleven parameters, each within the range $0 \leq x_1, \dots, x_{10} < 2\pi$ and $0 < y \leq 3$. Subsequently, we minimise the loss function through a series of iterations, with a total of $N_{\text{iter}} = 10^6$ iterations. This process enables us to collect 1024 samples of numerically optimised parameter sets.

Fig. 8 illustrates the minimised loss function values (averaged over the last 100 steps of the total $N_{\text{iter}} = 10^6$ iterations) and the corresponding optimised parameter y values. Among the 1024 samples, $\lesssim 10\%$ deviate to $y < 0$ (this numerical artefact arises from our definition of the loss function, Eqn. (55), which becomes zero at $y = -1$); these samples have been discarded. The distribution for y exhibits a peak around $y \approx 0.75$. This value differs from the 45-Higgs model ($y = 3$) or the 24-Higgs model ($y = 1.5$), but it aligns with the results presented in Sec. III C, which indicate the preference for the 24-Higgs model over the 45-Higgs model, as $y = 1.5$ is closer to $y \approx 0.75$. The group-theoretical reason for this value, $y \approx 0.75$, as

suggested by the machine learning approach, is unknown to us. Fig. 8 also indicates the appearance of another peak at $y \approx 1.3$. All three cases, x_0 : $x_0 = 0$, $2\pi/3$, and $4\pi/3$, give similar results, indicating these three values are equally natural by our criteria.

C. Supersymmetric scenario

The supersymmetric version of the generalised model is similar to above, except that the fermion mass data of the supersymmetric $SU(5)$, Eqs. (50) and (51), are utilised at the unification scale. Numerical optimisation of eleven parameters, x_1, \dots, x_{10} and y , is carried out with randomly generated initial values from the uniform distribution in the range $0 \leq x_1, \dots, x_{10} < 2\pi$ and $0 < y \leq 3$. We collected 1024 samples for each case of $x_0 = 0$, $2\pi/3$, and $4\pi/3$.

Fig. 9 illustrates the minimised loss function values (averaged over the last 100 steps of the total $N_{\text{iter}} = 10^6$ iterations) and the corresponding optimised parameter y values. A small fraction ($\lesssim 10\%$) of samples that resulted in negative values of y have been discarded as numerical artefacts. The distribution for y exhibits a peak around $y \approx 0.85$, which differs from the values representing the 45-Higgs model ($y = 3$) or the 24-Higgs model ($y = 1.5$). This value is nevertheless consistent with the results of Sec. IV C, as it is closer to the 24-Higgs model ($y = 1.5$) than the 45-Higgs model ($y = 3$). The group-theoretical reason for this optimal value, $y \approx 0.85$, is not known to us. There also appears to be a second peak at $y \approx 1.2$. The three values of x_0 , i.e. $x_0 = 0$, $2\pi/3$, and $4\pi/3$, give similar results and these values are deemed equally natural by our criteria.

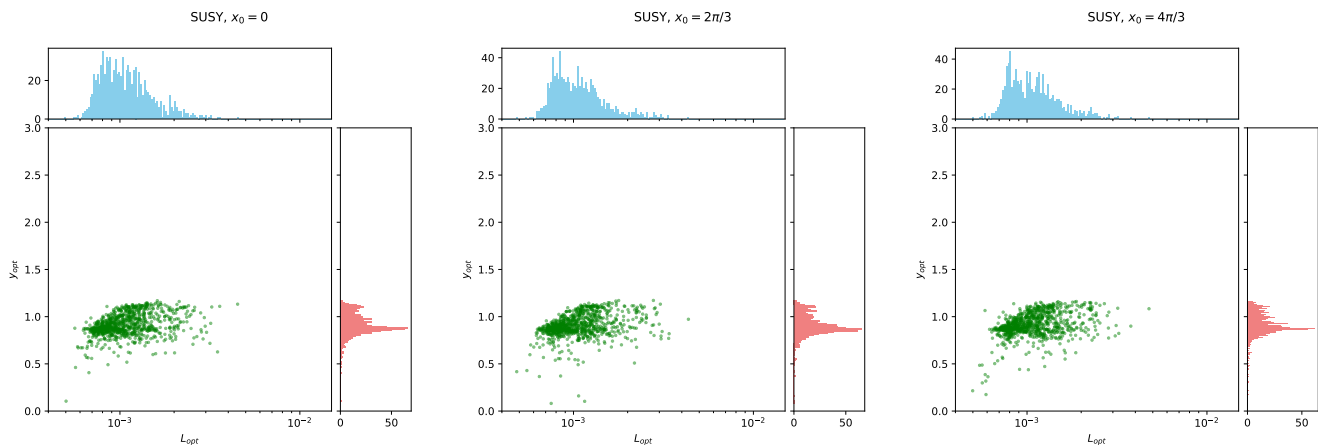


FIG. 9. Optimised values of the loss function and parameter y , for $x_0 = 0$ (left panel), $x_0 = 2\pi/3$ (middle) and $x_0 = 4\pi/3$ (right), in the generalised model of supersymmetric SU(5) GUT. Optimisation was conducted for iteration steps $N_{\text{iter}} = 10^6$ and 1024 samples were collected for each case. A small fraction ($< 10\%$) of samples resulted in $y < 0$ and were discarded. The optimised (minimised) loss function values are the average of the last 100 steps. The distribution of the optimised values for the loss function (light blue) and y (pink) are also presented in subplots.

VI. FINAL REMARKS

In this paper, we investigated the flavour sector of the SU(5) GUT using machine learning techniques. Phenomenologically viable SU(5) GUT models necessarily involve an enlarged Yukawa sector for which a comprehensive parameter scan is impractical. We focused on two well-known models, one involving the 45-dimensional Higgs field (45-Higgs model) and the other involving the 24-dimensional Higgs field (24-Higgs model), and compared these models in terms of naturalness, which we defined as the proximity to the original Georgi-Glashow model of SU(5) GUT. We first analysed the nonsupersymmetric model in which the grand unification is accomplished with the assistance of vectorlike fermions, then moved on to analyse the supersymmetric model. In both nonsupersymmetric and supersymmetric scenarios, our numerical studies indicated that the 24-Higgs model is closer to the Georgi-Glashow model. This implies that the 24-Higgs model is more natural, or more beautiful, than the 45-Higgs model.

Subsequently, we proposed a novel model that incorporates a one-parameter family, denoted as y , thereby extending the scope of these two models. Through a numerical optimisation process, we determined that the optimal value of y is approximately 0.75 in the nonsupersymmetric scenario, while it assumes a slightly higher value of approximately 0.85 in the supersymmetric scenario. Furthermore, we identified a secondary peak associated with the primary peak. In the nonsupersymmetric case, this secondary peak is characterised by a value of y approximately equal to 1.3, whereas in the supersymmet-

ric case, it is associated with a value of y approximately equal to 1.2.

The novel analysis presented here exemplifies the efficacy of machine learning techniques in the realm of high-energy physics beyond the Standard Model when conventional methodologies prove impractical. Furthermore, it raises several new questions. Numerical optimisation indicates that certain parameter values exhibit greater favourability in accordance with our criteria of naturalness. As evident from Figs. 5 and 7, certain regions are designated as favoured (dark) while others are unfavourable (blank). It would be of great interest to delve deeper into their phenomenological implications [25], particularly in the domains of neutrino physics, baryogenesis, and cosmological model construction [26–28]. In the generalised model introduced in Sec. V, the underlying physics behind the optimised parameter values $y \approx 0.75 - 0.85$ remains elusive. The 45-Higgs model posits the interplay of the 45-Higgs field, whereas the 24-Higgs model introduces higher-dimensional (non-renormalisable) operators, thereby delineating distinct physical origins. These two mechanisms can coexist, yet comprehending the specific values attained by the optimised parameter y may necessitate a larger, possibly ultraviolet-complete, framework encompassing these models.

ACKNOWLEDGMENTS

This work was supported in part by the United States Department of Energy Grant Nos. DE-SC0012447, DE-SC0023713, and DE-SC0026347 (N.O.).

-
- [1] G. Aad *et al.* (ATLAS), Observation of a new particle in the search for the Standard Model Higgs boson with the ATLAS detector at the LHC, Phys. Lett. B **716**, 1 (2012), arXiv:1207.7214 [hep-ex].
- [2] S. Chatrchyan *et al.* (CMS), Observation of a New Boson at a Mass of 125 GeV with the CMS Experiment at the LHC, Phys. Lett. B **716**, 30 (2012), arXiv:1207.7235 [hep-ex].
- [3] B. P. Abbott *et al.* (Virgo, LIGO Scientific), Observation of Gravitational Waves from a Binary Black Hole Merger, Phys. Rev. Lett. **116**, 061102 (2016), arXiv:1602.03837 [gr-qc].
- [4] Y.-H. He, Machine-learning the string landscape, Phys. Lett. B **774**, 564 (2017).
- [5] J. Halverson, B. Nelson, and F. Ruehle, Branes with Brains: Exploring String Vacua with Deep Reinforcement Learning, JHEP **06**, 003, arXiv:1903.11616 [hep-th].
- [6] K. T. Matchev, K. Matcheva, P. Ramond, and S. Verner, Exploring the truth and beauty of theory landscapes with machine learning, Phys. Lett. B **856**, 138941 (2024), arXiv:2401.11513 [hep-ph].
- [7] T. R. Harvey and A. Lukas, Quark Mass Models and Reinforcement Learning, JHEP **08**, 161, arXiv:2103.04759 [hep-th].
- [8] S. Nishimura, C. Miyao, and H. Otsuka, Exploring the flavor structure of quarks and leptons with reinforcement learning, JHEP **23**, 021, arXiv:2304.14176 [hep-ph].
- [9] F. A. de Souza, M. Crispim Romão, N. F. Castro, M. Nikjoo, and W. Porod, Exploring parameter spaces with artificial intelligence and machine learning black-box optimization algorithms, Phys. Rev. D **107**, 035004 (2023), arXiv:2206.09223 [hep-ph].
- [10] J. C. Romão and M. Crispim Romão, Combining evolutionary strategies and novelty detection to go beyond the alignment limit of the Z3 3HDM, Phys. Rev. D **109**, 095040 (2024), arXiv:2402.07661 [hep-ph].
- [11] H. Georgi and S. L. Glashow, Unity of All Elementary Particle Forces, Phys. Rev. Lett. **32**, 438 (1974).
- [12] J. R. Ellis and M. K. Gaillard, Fermion Masses and Higgs Representations in SU(5), Phys. Lett. B **88**, 315 (1979).
- [13] H. Georgi and C. Jarlskog, A New Lepton - Quark Mass Relation in a Unified Theory, Phys. Lett. B **86**, 297 (1979).
- [14] S. Kawai and N. Okada, Truth, beauty, and goodness in grand unification: A machine learning approach, Phys. Lett. B **860**, 139221 (2025), arXiv:2411.06718 [hep-ph].
- [15] T. Ohlsson and M. Pernow, Running of Fermion Observables in Non-Supersymmetric SO(10) Models, JHEP **11**, 028, arXiv:1804.04560 [hep-ph].
- [16] C. Abel *et al.*, Measurement of the Permanent Electric Dipole Moment of the Neutron, Phys. Rev. Lett. **124**, 081803 (2020), arXiv:2001.11966 [hep-ex].
- [17] P. H. Frampton and S. L. Glashow, Staying Alive With SU(5), Phys. Lett. B **131**, 340 (1983), [Erratum: Phys.Lett.B 135, 515 (1984)].
- [18] U. Amaldi, W. de Boer, P. H. Frampton, H. Furstenau, and J. T. Liu, Consistency checks of grand unified theories, Phys. Lett. B **281**, 374 (1992).
- [19] D. Buttazzo, G. Degrandi, P. P. Giardino, G. F. Giudice, F. Sala, *et al.*, Investigating the near-criticality of the Higgs boson, JHEP **1312**, 089, arXiv:1307.3536 [hep-ph].
- [20] K. Abe *et al.* (Super-Kamiokande), Search for proton decay via $p \rightarrow e^+ \pi^0$ and $p \rightarrow \mu^+ \pi^0$ in 0.31 megaton-years exposure of the Super-Kamiokande water Cherenkov detector, Phys. Rev. D **95**, 012004 (2017), arXiv:1610.03597 [hep-ex].
- [21] N. Haba, Y. Mimura, and T. Yamada, Proton Lifetime Upper Bound in Non-SUSY SU(5) GUT, Phys. Rev. D **99**, 075018 (2019), arXiv:1812.08521 [hep-ph].
- [22] D. P. Kingma and J. Ba, Adam: A Method for Stochastic Optimization (2014) arXiv:1412.6980 [cs.LG].
- [23] S. Navas *et al.* (Particle Data Group), Review of particle physics, Phys. Rev. D **110**, 030001 (2024).
- [24] D. J. Castano, E. J. Piard, and P. Ramond, Renormalization group study of the Standard Model and its extensions. 2. The Minimal supersymmetric Standard Model, Phys. Rev. D **49**, 4882 (1994), arXiv:hep-ph/9308335.
- [25] I. Doršner and S. Saad, Is doublet-triplet splitting necessary?, Phys. Rev. D **110**, 075025 (2024), arXiv:2404.09021 [hep-ph].
- [26] A. H. Guth, The Inflationary Universe: A Possible Solution to the Horizon and Flatness Problems, Phys. Rev. D **23**, 347 (1981).
- [27] M. Arai, S. Kawai, and N. Okada, Higgs inflation in minimal supersymmetric SU(5) GUT, Phys. Rev. D **84**, 123515 (2011), arXiv:1107.4767 [hep-ph].
- [28] S. Kawai and J. Kim, Multifield dynamics of supersymmetric Higgs inflation in SU(5) GUT, Phys. Rev. D **93**, 065023 (2016), arXiv:1512.05861 [hep-ph].